

RESEARCH ARTICLE

Woody and herbaceous invasive alien plant species-derived biochars are potentially optimal for soil amendment, soil remediation, and carbon storage

Alex Ceriani¹ | Michele Dalle Fratte¹ | Gustavo Agosto¹ | Peter Beatrice¹ |
 Marcella Reguzzoni² | Lorenzo Bettucci³ | David Casini³ |
 Bruno Enrico Leone Cerabolini¹ | Antonio Montagnoli¹

¹Department of Biotechnology and Life Science, University of Insubria, Varese, Italy

²Department of Medicine and Surgery, University of Insubria, Varese, Italy

³Re-Cord, Renewable Energy Consortium for R&D, Florence, Italy

Correspondence

Michele Dalle Fratte, Department of Biotechnology and Life Science, University of Insubria, via Dunant 3, Varese, Italy.

Email: michele.dallefratte@uninsubria.it and michele.dallefratte@gmail.com

Funding information

Fondazione Lombardia per l'Ambiente; Italian Ministry of University and Research

Abstract

Invasive alien plant species (IAPS) are a global problem, representing a threat to ecosystem functioning, biodiversity, and human health. Legislation requires the management and eradication of IAPS populations; yet, management practices are costly, require several interventions, and produce large amounts of waste biomass. However, the biomass of eradicated IAPS can become a resource by being used as feedstock for biochar production and, at the same time, implementing the management of IAPS. Here we carried out an in-depth characterization of biochar produced at 550°C derived from 10 (five woody and five herbaceous) widespread IAPS in the central-southern Alps region to determine their potential applications for soil amendment, soil remediation, and carbon storage. Biochar was produced at a laboratory scale, where its physicochemical characteristics, micromorphological features, and lead adsorption from aqueous solutions were measured. To investigate any possible trade-offs among the potential biochar applications, a principal component analysis was performed. IAPS-derived biochars exhibited relevant properties in different fields of application, suggesting that IAPS biomass can be exploited in a circular economy framework. We found coordinated variation and trade-offs from biochars with high stability to biochars with high soil amendment potential (PC1), while the biochar soil remediation potential represents an independent axis of variation (PC2). Specifically, IAPS-derived biochar had species-specific characteristics, with differences between the woody and herbaceous IAPS, the latter being more suitable for soil amendment due to their greater pH, macronutrient content, and macropore area. Biochar derived from woody IAPS showed a greater surface area, smaller pores, and had higher lead adsorption potentials from aqueous solutions, hinting at their higher potential for heavy metal pollution remediation. Moreover, biochar derived from woody IAPS had a higher fixed carbon content, indicating higher carbon stability,

This is an open access article under the terms of the [Creative Commons Attribution](https://creativecommons.org/licenses/by/4.0/) License, which permits use, distribution and reproduction in any medium, provided the original work is properly cited.

© 2024 The Authors. *GCB Bioenergy* published by John Wiley & Sons Ltd.

and suggesting that their biochar is preferable for carbon sequestration in the view of climate change mitigation.

KEYWORDS

biological invasion management, carbon negative, globalization, soil amendment, soil remediation, sustainability

1 | INTRODUCTION

The 21st century is facing the problem of the rise of biological invasion following the increase of globalization (Barney et al., 2013), to such an extent that the term Exocene has been used to characterize this historical era (Bolpagni, 2021). An increasing number of invasive alien plant species (IAPS) have become dominant in newly colonized areas (Haubrock et al., 2021), causing widespread negative impacts on biodiversity and ecosystem functioning (Pérez et al., 2022). IAPS are naturalized plants that produce reproductive offspring at considerable distances from the parent plant and then have the potential to spread over large areas (Pyšek et al., 2004). Compared to native species, many IAPS have higher growth rates, larger sizes, and are likely to allocate more biomass (Kaushik et al., 2022; Van Kleunen et al., 2010; Zanzottera et al., 2021). Also, with the rapid change in climate, IAPS may find more favorable conditions in which they can spread (Dimitrova et al., 2022; Pérez et al., 2022), thus becoming increasingly dominant in the host environment. IAPS eradication and management is mandatory worldwide (e.g., EU Regulation 1143/2014; US Executive Order 13751/2016; New Zealand's Biosecurity Act 1993 and Biosecurity Strategy 2003; Australia's Environment Protection and Biodiversity Conservation Act 1999). However, management efforts are often ineffective, require continuous implementation, and are expensive (Borokini & Babalola, 2012; Diagne et al., 2021; Haubrock et al., 2021). The eradicated biomass is considered a waste to be disposed of, but its valorization could help cut these costs. Nonetheless, since IAPS produces a large amount of readily available biomass, avoiding land conversion and competition with food, its biomass may represent a sustainable feedstock for different applications, ranging from bioenergy production to bio-based materials (Carson et al., 2018; Ceriani et al., 2023; Mathew & Saravanakumar, 2022; Monteiro & Ferreira, 2022; Nackley et al., 2013; Velvizhi et al., 2022). This concept is crucial within the EU's "Next Generation EU" project (<https://next-generation-eu.europa.eu>) to achieve the goal of climate neutrality.

Biomass' complex and recalcitrant three-dimensional molecular structures complicates treatments necessary

to obtain the desired end products (Velvizhi et al., 2022). One such treatment is pyrolysis, where a thermochemical decomposition process occurs with little or no oxygen at high temperatures, obtaining three different phase products (liquid, solid, and gaseous). Biochar represents the solid phase of pyrolysis and is characterized by great carbon content, porous structure, surface area (SA), and high richness of functional groups (Ni et al., 2020; Weber & Quicker, 2018; Yaashikaa et al., 2020). These properties can be tailored to a specific use by selecting the feedstock and pyrolysis conditions (e.g., temperature, heating rate, and residence time) (Weber & Quicker, 2018). Many biochar properties are temperature dependent for example, an increase in pyrolysis temperature is usually related to higher SA and pH values due to the volatilization of acidic functional groups (OH and COOH), and the accumulation of inorganic salts, and carbonates (Ippolito et al., 2020; Weber & Quicker, 2018; Yuan et al., 2011). However, biochar mass yields are higher at lower temperatures because of the release of volatile matter from the biomass (Wang et al., 2021). Cation exchange capacity (CEC) is also highest in biochars produced at relatively low temperatures, where the SA has increased significantly compared to feedstocks and at the same time retains sufficient functional groups to provide negative charges (Weber & Quicker, 2018). In addition, it has been observed that the temperature range where pore volume increased was between 250 and 500°C and decreased as the temperature increased from 550 to 750°C (Ni et al., 2020). 550°C, hence, is a temperature at which the trade-offs between the different biochar temperature-dependent characteristics are optimal, thus representing an ideal temperature to investigate the properties of biochars from feedstocks that have not yet been measured. What is more, above this temperature, some biochar parameters, such as fixed carbon, carbon, oxygen, and aromaticity, as well as the metal removal, do not drastically change (Chi et al., 2017; Weber & Quicker, 2018).

Therefore, according to its characteristics, biochar results in a versatile product-material that can have a wide spectrum of applications, ranging from agriculture as a soil amendment to soil pollutant stabilization, assisting phytoremediation, and carbon storage (Amalina et al., 2022). Indeed, there is ample evidence that biochar

stimulates plant growth of different crop species and wild plants (Baronti et al., 2022; Montagnoli et al., 2021) and that its structure and physicochemical properties can favor the absorption of heavy metals present in contaminated soils (Nandillon, Lebrun, et al., 2019; Nandillon, Miard, et al., 2019). Moreover, the high carbon stability of biochar determines its potential for carbon sequestration when incorporated into the soil (Leng et al., 2019). These properties have only recently begun to be tested on IAPS-derived biochar (e.g., Fan et al., 2019; Feng et al., 2021; Liu et al., 2022). Indeed, the conventional feedstock for biochar production is fill material, straw, and wood waste (Wang et al., 2021). However, the biomass of eradicated IAPS seems promising as feedstock for biochar production (Feng et al., 2021). Considering the large area invaded by IAPS and the costs associated with the disposal of their eradicated biomass, using IAPS to produce biochar would help meet sustainability goals and improve IAPS management practices (Liao et al., 2013). Also, since the parent material is one of the main factors determining biochar properties (Weber & Quicker, 2018), IAPS biomass can have high heterogeneity with a wide range of functional groups (Dalle Fratte et al., 2019; Ferraro et al., 2021), making crucial the characterization of IAPS-derived biochar to pinpointing its optimal end use, greatly enhancing IAPS management, and circular economy perspectives, supporting the notion that IAPS management would benefit from the valorization of its eradicated biomass.

Our work aimed to determine whether biochar produced from IAPS biomass, resulting from the eradication imposed by law, can have desirable properties for (i) soil amendment, (ii) soil remediation of heavy metals, and (iii) carbon sequestration. To this end, we investigated the physicochemical, morphological, and functional properties of biochar derived from five woody and five herbaceous IAPS most widespread in the central-southern Alps, for which an in-depth characterization has never been performed. We also analyzed lead absorption from an aqueous solution and investigated the differences between the growth forms.

2 | MATERIALS AND METHODS

2.1 | IAPS selection and biomass sampling

We selected five herbaceous (*Artemisia verlotiorum*, *Ludwigia grandiflora*, *Pueraria lobata*, *Reynoutria japonica*, and *Solidago gigantea*) and five woody (*Ailanthus altissima*, *Buddleja davidii*, *Prunus serotina*, *Quercus rubra*, and *Trachycarpus fortunei*) IAPS with the highest

ecological impact in the Lombardy administrative region (northern Italy, central-southern Alps) based on their occurrence in grid cells of 10×10 km² (Bisi et al., 2018). These IAPS were all listed in the regional blacklist of the Lombardy region (regional law 31/2008); hence, their eradication is mandatory. For each of these IAPS, during the 2022 growing season, we randomly collected 3 kg ca. of aboveground biomass fresh weight (leaf, stem, and branches); specifically, six plants per species were collected and considered independent replicates (in the case of *L. grandiflora*, roots were included). Plants were collected from highly invaded sites located at similar altitudes and at a great distance from potential anthropic disturbances that could impact biomass nutrient content. The biomass was first chipped (~7 cm²; woodchipper GeoTech PCS70L) and then pre-dried in an aerated room for 10 days at a mean temperature of 25°C. The six plants of each species were gathered in a pool sample, where subsamples were finally oven-dried at 80°C for 24 h (until constant weight) and milled (4 mm mesh; mill Retsch SM 300) for biochar production. The obtained biochar was then used for the measurement in triplicate of the different properties.

2.2 | Biochar production

For each of the 10 IAPS, a biomass subsample was collected for biochar production. Biochar was prepared using a macro TGA (LECO TGA 701) under nitrogen flow (10 L min⁻¹) at 550°C for 1 h (heating rate of 20°C min⁻¹). We calculated the biochar yield using the following equation:

$$\text{Yield (\%)} = (\text{grams of biochar} / \text{grams of feedstock}) \times 100.$$

2.3 | Biochar analysis

2.3.1 | Physicochemical properties

Ultimate analysis (carbon [C], hydrogen [H], and nitrogen [N] content) was performed using subsamples of 60–80 mg in three replicates of each IAPS biochar using a flash combustion procedure (LECO TruSpec CHN instrument). The oxygen (O) content was calculated using the following mass balance equation (Ferraro et al., 2021):

$$\text{O (\%)} = 100(\%) - \text{C (\%)} - \text{H (\%)} - \text{N (\%)} - \text{Ash (\%)}.$$

H:C_{org} and O:C_{org} molar ratios were also calculated considering the organic carbon content. The organic carbon (C_{org}) was measured using a calcimeter (Sherrod et al., 2002), where 1 g of biochar reacted with HCl (34%–37%), releasing CO₂, which was used to obtain the grams of CaCO₃ in the sample using the formula 0.0045×CO₂

(mL) – 0.0127. The grams of CaCO_3 were then divided by the total weight of the sample to obtain the percentage of CaCO_3 and by multiplying this value by 0.12 (the amount of carbon in CaCO_3), the percentage of total inorganic carbon was obtained (Appendix S1). This measurement was then subtracted from the total C (%) to obtain C_{org} (%).

Macronutrients such as magnesium (Mg), potassium (K), phosphorus (P), and calcium (Ca) total content were measured in three technical replicas of 0.05 g for each species using an inductively coupled plasma mass spectrometry (ICP Agilent 4200 MP-AES) instrument. Before measurements, each sample was first mineralized in a Teflon vessel of a microwave digester with a 3 mL H_2O_2 36% and 8 mL HNO_3 67% solution. Then the samples were diluted with HNO_3 up to 20 mL of volume for ICP measurement.

Proximate analysis (ash, volatile matter, moisture, and fixed carbon content) was conducted using the LECO TGA 701 instrument. Ash, volatile matter, and moisture contents were estimated based on three replicas of 1 g for each species. Samples were heated at 900°C for 7 min (10 L min^{-1} nitrogen flow) or at 105°C until constant weight (5 L min^{-1} airflow) to estimate volatile matter content, ash content, and moisture content, respectively. To calculate each parameter, we used the following formulas:

$$\text{Ash (\%)} = (\text{Ash mass} / \text{Initial mass}) \times 100.$$

Volatile matter (%)

$$= (\text{Moisture weight} - \text{Volatile weight}) / \text{Initial mass} \times 100.$$

Moisture content (%)

$$= (\text{Initial weight} - \text{Moisture weight}) / \text{Initial mass} \times 100.$$

The percentage of fixed carbon was calculated based on the balance equation (Corton et al., 2016):

$$\text{Fixed carbon (\%)} = 100 - (\text{Moisture} + \text{Volatile} + \text{Ash}).$$

For SA and porosity measurements, 60 mg of biochar were dried at 200°C for 48 h and then degassed at 200°C for 24 h under a vacuum. The SA was measured by N_2 adsorption isotherms at 77 K by applying the Brunauer–Emmett–Teller equation (BET) in a Quantachrome NOVA 2200E instrument.

pH was measured using a digital pH meter (Mettler Toledo FiveEasy Plus) in a 1:5 (volume fraction) suspension of biochar in water.

The lead (Pb) adsorption capacity was measured in aqueous solutions in three replicates (Chi et al., 2017). We added 0.02 g of each biochar sample to a 50-mL flask containing 20 mL of Pb^{2+} solution (20 mg/L) prepared with $\text{Pb}(\text{NO}_3)_2$. The falcon tubes were subjected to a shaker at a speed of 150 rpm for 24 h at room temperature. The solutions were then filtered to remove any solid residue

of biochar. The filtered solutions were analyzed through a flame atomic absorption spectrometer, and the remaining lead content in the solution was recorded. This was used to calculate the percentage of Pb^{2+} removed from the solution: [percentage removed (%) = $(C_0 - C_1) / C_0 \times 100\%$], where C_0 represents the original concentration and C_1 is the remaining concentration.

Cation exchange capacity was measured in three replicates using the barium chloride compulsive exchange method (Skjemstad et al., 2008). Two grams of biochar were saturated with a barium chloride solution. The samples were then treated with magnesium sulfate, which allowed the barium to deposit as insoluble barium sulfate and exchange with magnesium. After recovering this solution, a titration procedure with EDTA was performed to quantify the amount of magnesium exchanged, and hence the CEC value was determined as follows:

$$\text{CEC} = (\text{VB} - \text{VA}) \times 0.25 \times (30 + B - A) / M,$$

where VB is the volume of the solution of EDTA used to titrate the blank solution (mL), VA is the volume of the solution of EDTA used to titrate the sample solution (mL), B is the mass of the falcon tube after the sample was washed with H_2O (g), A is the mass of the falcon tube plus sample before the washing with BaCl_2 (g), and M is the mass of the biochar sample (g).

Fourier infrared spectroscopy (FT-IR) analysis was performed to determine surface functional groups using a SHIMADZU IRTracer-100 spectrometer. The spectral range investigated was from 600 to 4000 cm^{-1} . A total of 45 scans were averaged to have an acceptable signal-to-noise ratio. The analysis was also performed on feedstock samples to compare the spectra with those of the corresponding biochar.

2.3.2 | Micromorphological properties

Biochar's microporosity was estimated using the density functional theory approach on BET isotherms. To analyze macropore area distribution, we embedded biochar fragments in Technovit 7100 resin (Kulzer GmbH, Germany) and placed them under a vacuum so that the resin could penetrate the pores. Samples were sliced with a Leica SM 2400 microtome (Leica Biosystems, Germany) at a thickness of $12\text{ }\mu\text{m}$ and photographed using an Olympus BX63 optical microscope equipped with an Olympus DP72 camera (Olympus Scientific Solutions, Japan) to observe the biochar cross-section anatomy at a $10\times$ magnification (Appendix S1). Digital images were analyzed with cellSens imaging software (Olympus). Pore area of the cross-section of three biochar images per species was estimated using ImageJ (Schneider et al., 2012) software.

To assess the overall biochar morphology, scanning electron microscopy (SEM) images were acquired using a PHILIPS XL30 FEG instrument. The samples were placed on an aluminum stand using conductive carbon adhesive tape. The metallization of the biochar (at 15 mA for 45 s) was performed before observations to improve the resulting images. The acceleration voltage of the electron beam was 5 kV. Images were taken at a magnification of 1000 \times to highlight biochar's macrostructure.

2.4 | Statistical analysis

The statistical analysis was conducted using the R studio software (R Core Team, 2022). We checked for the unimodal distribution of data using the function “Shapiro.test” from the “stats” base R package (Shapiro & Wilk, 1965), and where the unimodal assumption was not met, data were log-transformed. An ANOVA test with the “aov” function was performed for the statistical analysis from the “stats” base R package. To compare differences among different IAPS and between herbaceous and woody growth forms, we used the Tukey post-hoc comparison by means of the function “TukeyHSD” of the “stats” base R package. We then performed a principal component analysis (PCA) on all the variables describing the properties of soil amendment, remediation, and carbon storage to investigate trade-offs among the potential biochar applications. We then tested the correlation among the selected variables and the significant components of the PCA using the “chart.Correlation” function from the package “PerformanceAnalytics” (Peterson et al., 2022). Data were log-transformed, centered, and scaled before running the PCA, which was done using the “principal” function in the package “psych” (Revelle, 2023).

3 | RESULTS

3.1 | Physicochemical properties

Carbon (C) content was significantly higher in woody IAPS (mean = 84.59%) compared to herbaceous ones (73.96%) (Figure 1A). The C value was the same for all woody IAPS, but we observed significant differences among herbaceous ones, with the highest C values being those of *A. verlotiorum* and *S. gigantea* (respectively 79.39% and 79.30%) and the lowest being those of *P. lobata* (65.71%) (Figure 1B). Similarly, hydrogen (H) and oxygen (O) contents were higher in woody IAPS (being respectively 2.53% and 5.70%) compared to herbaceous ones (1.92% and 2.33%) (Figure 1C,E).

The highest H value was observed for *B. davidii*, *P. serotina*, and *Q. rubra* (mean value ranging from 2.63% to 2.74%), as opposed to *P. lobata* and *R. japonica*, which had the lowest H values (respectively 1.81% and 1.77%) (Figure 1D). The highest O value was that of *B. davidii*, *P. serotina*, and *Q. rubra* (from 6.13% to 7.72%), while *P. lobata*, *R. japonica*, and *S. gigantea* had the lowest O values (from 1.26% to 1.52%) (Figure 1F). Nitrogen (N) content (Figure 1G,H) was significantly higher in herbaceous IAPS (2.10%) compared to woody ones (1.03%). *L. grandiflora*, *P. lobata*, and *R. japonica* had the highest N values (from 2.19% to 2.79%), followed by *A. verlotiorum*, and *S. gigantea*, which in turn had similar N values to *T. fortunei*, while the lowest value was that of *Q. rubra* (0.81%).

The H:C_{org} ratios vary between 0.3 and 0.4 (Figure 1I,J), with woody species having higher ratios (Figure 1I). *Q. rubra*'s biochar showed the highest value, along with *P. serotina* and *B. davidii* (ranging from 0.37 to 0.39), whereas *R. japonica*'s biochar had the lowest overall value (0.29) (Figure 1J). The O:C_{org} ratio ranged between 0.02 and 0.08 (Figure 1K,L), with woody species having higher values (Figure 1K). Here too, *Q. rubra*'s showed the highest value (0.07) and *R. japonica*'s biochar presented the lowest one (0.01), along with *S. gigantea* (Figure 1L).

Herbaceous IAPS-derived biochars showed higher concentrations of calcium (Ca), potassium (K), magnesium (Mg), and phosphorus (P) in comparison to those derived by woody IAPS (Figure 1M,O,Q,S). K was the macronutrient with the highest concentration in both herbaceous and woody IAPS-derived biochars (the average value being, respectively, 41691.14 and 17279.73 mg kg⁻¹) (Figure 1O,P), the second most abundant was Ca (respectively, 28976.89 and 9452.36 mg kg⁻¹) (Figure 1M,N), and the macronutrient with the lowest concentration was P (respectively, 4483.49 and 1428.75 mg kg⁻¹) (Figure 1S,T). The biochar with the highest Ca concentration was that of *P. lobata* (46460.95 mg kg⁻¹), contrary to that of *P. serotina*, which showed the lowest value (4481.12 mg kg⁻¹). The biochar with the highest K concentration was that of *R. japonica* (60598.82 mg kg⁻¹), while the one with the lowest was that of *P. serotina* (6262.42 mg kg⁻¹). *P. lobata* had the highest Mg concentration (9472.97 mg kg⁻¹), and *P. serotina* had the lowest (1109.62 mg kg⁻¹). Considering P biochars with the highest concentrations were *R. japonica*, *L. grandiflora*, and *A. verlotiorum* (from 4878.49 to 6107.52 mg kg⁻¹), *Q. rubra* had the lowest (163.55 mg kg⁻¹).

Herbaceous IAPS had higher average yields than woody ones, being respectively 29.27% and 24.66% (Figure 2A). Among herbaceous IAPS, *L. grandiflora* and *S. gigantea* exhibited, respectively, the highest and the lowest yields, being respectively 34.59% and 26.71%. Among woody species, *T. fortunei* and *B. davidii* (respectively, 26.66% and

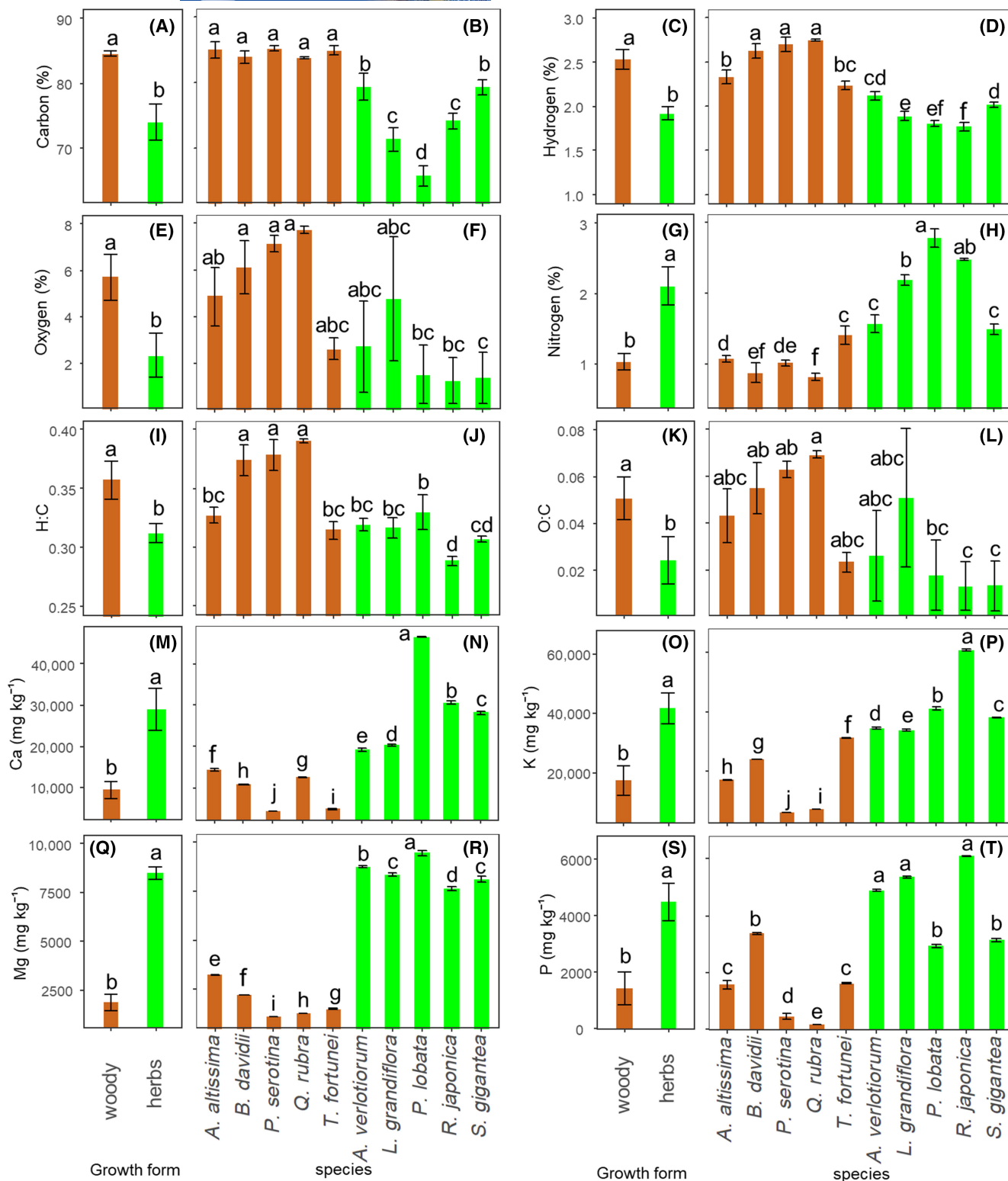


FIGURE 1 Data represent the mean of three replicates ($n=3$) and standard error of carbon (%) (A, B), hydrogen (%) (C, D), oxygen (%) (E, F), nitrogen (%) (G, H), H:C (I, J), O:C (K, L), Ca (mg kg^{-1}) (M, N), K (mg kg^{-1}) (O, P), Mg (mg kg^{-1}) (Q, R) and P (mg kg^{-1}) (S, T) of invasive alien plant species-derived biochar, grouped by growth forms (A, C, E, G, I, K, M, O, Q, S) and species (B, D, F, H, J, L, N, P, R, T). Small letters indicate post-hoc comparisons at $p < 0.05$.

26.53%) showed the highest yield, comparable to that of *S. gigantea*, while *Q. rubra* displayed the lowest yield (22.72%) (Figure 2B).

Proximate analyses are presented in Figure 2C–J. The ash content was higher in herbaceous IAPS compared to woody ones, being respectively 19.71% and

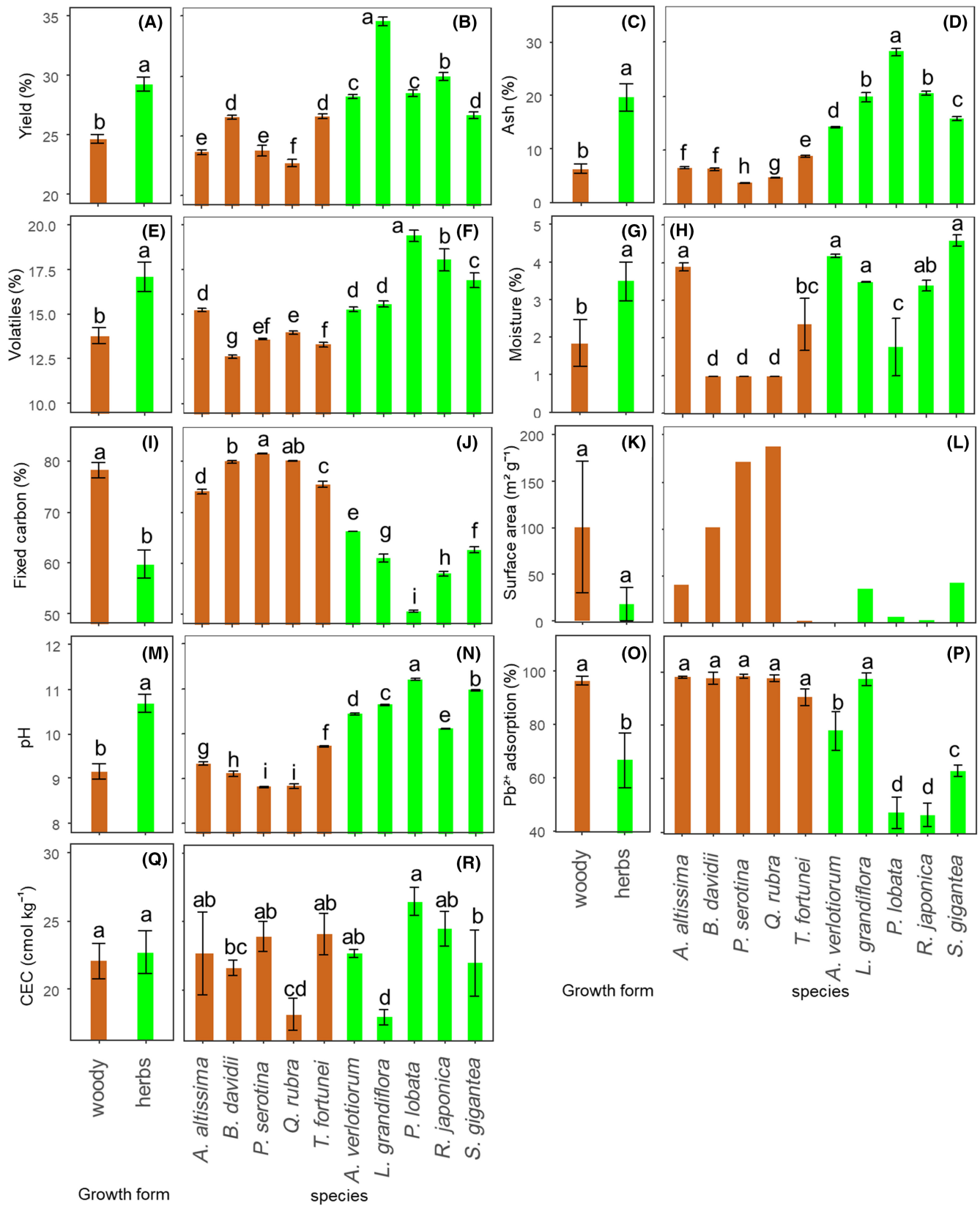


FIGURE 2 Data represent the mean of three replicates ($n = 3$) and standard error values of yield (%) (A, B), ash (%) (C, D), volatiles (%) (E, F), moisture (%) (G, H), fixed carbon (%) (I, J), surface area ($\text{m}^2 \text{g}^{-1}$) (K, L), pH (M, N), adsorbed Pb^{2+} (%) (O, P), and CEC (cmol g^{-1}) (Q, R) of invasive alien plant species-derived biochar, grouped by growth form (A, C, E, G, I, K, M, O, Q) and species (B, D, F, H, J, L, N, P, R). Small letters indicate post-hoc comparisons at $p < 0.05$. CEC, cation exchange capacity.

6.17% (Figure 2C). The highest ash value was recorded for *P. lobata* (28.18%), and the lowest was measured for *P. serotina* (3.96%). Similarly, volatiles and moisture content were higher in herbaceous IAPS (Figure 2E,G). The highest volatile content was recorded for *P. lobata* (19.44%); *A. altissima*-derived biochar had similar values to *L. grandiflora* and *A. verlotiorum* (15.60% and 15.29%), while the lowest was that of *B. davidii* (12.68%) (Figure 2F). Biochar's moisture content was highest in *A. altissima*, *A. verlotiorum*, *L. grandiflora*, and *S. gigantea* (from 3.49 to 4.61%). *B. davidii*, *P. serotina*, and *Q. rubra* had the lowest values (0.98%) (Figure 2H). Woody IAPS had significantly higher fixed carbon values compared to herbaceous ones, being respectively 78.21% and 59.73% (Figure 2I), with the highest recorded value for *P. serotina*, *Q. rubra*, and *B. davidii* (from 79.92% to 81.43%). The lowest fixed carbon values were recorded for *P. lobata* (50.61%) (Figure 2J).

On average, woody IAPS had a higher SA compared to herbaceous ones, although with no statistical differences (Figure 2K), with *Q. rubra* (187.70 m² g⁻¹) and *A. verlotiorum* (1.31 m² g⁻¹) having respectively the highest and the lowest values (Figure 2L). Among woody IAPS, *T. fortunei* showed the lowest SA (2.79 m² g⁻¹). On the other hand, some herbaceous IAPS (*L. grandiflora* and *S. gigantea*, respectively, 36.99 and 42.83 m² g⁻¹) had similar values to those observed for *A. altissima* (40.48 m² g⁻¹).

All biochar's pH was alkaline (Figure 2M,N), with herbaceous IAPS having significantly higher values compared to woody ones, being respectively 10.68 and 9.16 (Figure 2M), *P. lobata* had the highest value (11.22), and the lowest values were recorded for *P. serotina* (8.81) and *Q. rubra* (8.83) (Figure 2N).

The biochar lead (Pb²⁺) adsorption capacity from an aqueous solution was higher in woody IAPS than herbaceous ones, respectively 97.47% and 66.39% (Figure 2O). Among woody IAPS, the average biochar Pb²⁺ adsorption capacity was high (97%–98%) except for *T. fortunei*, whose biochar adsorbed on average 90.59% of Pb²⁺ from the aqueous solution, although without significant differences compared to other woody IAPS (Figure 2P). The Pb²⁺ adsorption capacity of biochar derived from herbaceous IAPS showed more heterogeneous results, being higher for *L. grandiflora* (97.41%), whose value was similar to that of woody IAPS, and lower for *P. lobata* (47.25%) and *R. japonica* (46.40%) (Figure 2P).

Considering the CEC, no significant differences were observed between woody and herbaceous IAPS-derived biochars, whose average values were respectively 22.09 and 22.71 cmol kg⁻¹ (Figure 2Q). However, we observed differences among the 10 IAPS: the highest measured CEC value was for *P. lobata*-derived biochar (26.48 cmol kg⁻¹),

followed by *R. japonica*, *T. fortunei*, *P. serotina*, *A. altissima*, and *A. verlotiorum*-derived biochars. The lowest value was observed for *L. grandiflora*-derived biochars (18.01 cmol kg⁻¹) (Figure 2R).

The IAPS-derived biochar showed similar overall stretching of the transmittance FT-IR spectra, particularly in the 2500–4000 cm⁻¹ range where the bands tended to flatten out (Figure 3a–j). Most of the variation of the bands concentrated in the 700–2000 cm⁻¹ range, with recognizable peaks in all 10 spectra. Specifically, the peaks were detected in the 750–900 cm⁻¹ regions corresponding to aromatic C–H out-of-plane deformation, 1110–1380 cm⁻¹, which relate to C–O and CH₂ vibrations, and the 1600–1700 cm⁻¹ regions, which correspond to C=C and C–O functional groups. A peak was also recognizable at 1420 cm⁻¹ relating to inorganic CO₃²⁻. The spectra of IAPS's biomass have peaks that are not observable in the biochar ones. These peaks are at 1000 cm⁻¹, relating to C–O, C–C stretching, and C–OH bending; 2900, and 3420 cm⁻¹, which are associated with C–O–H or C–O–R groups (Figure 3a–j).

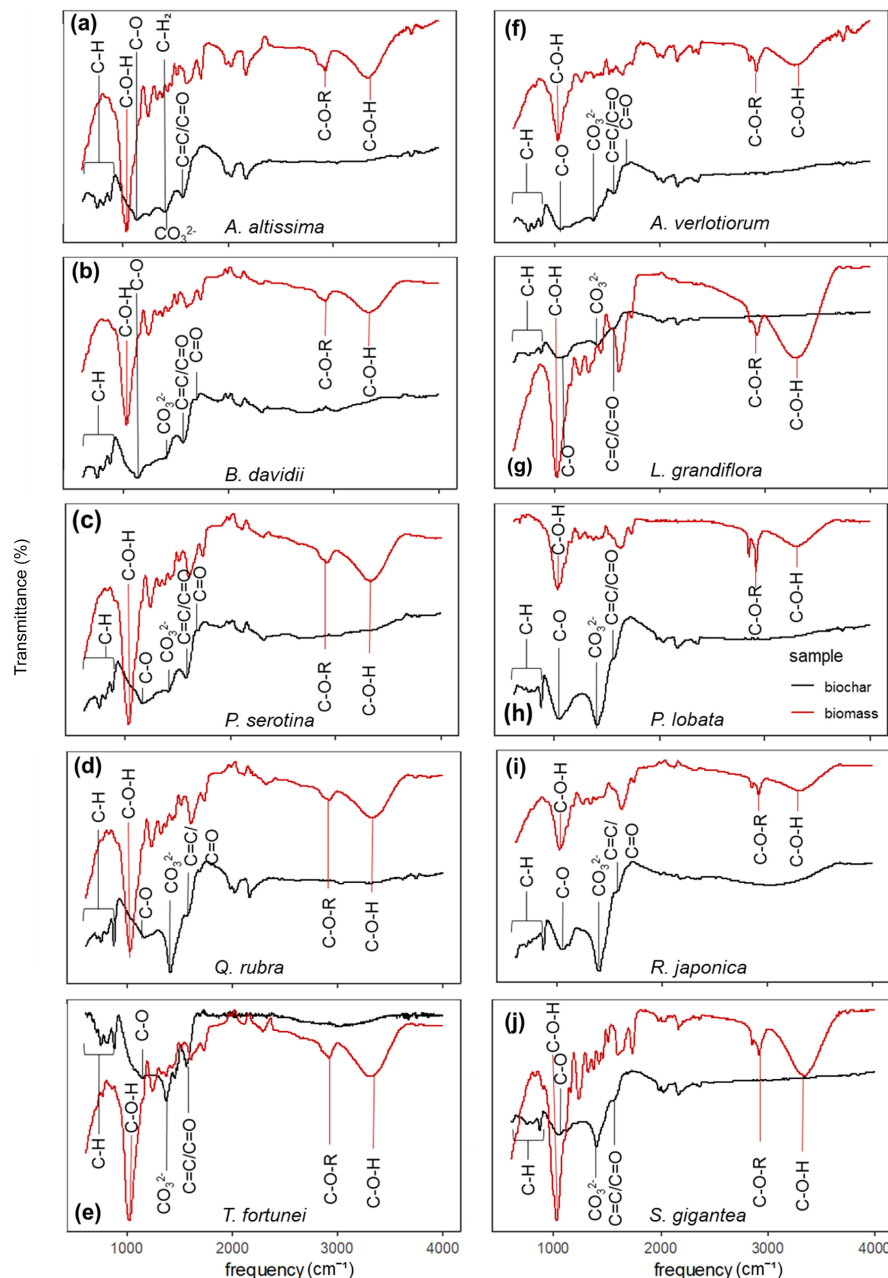
3.2 | Micromorphological properties

The micropores of the biochar derived from woody and herbaceous IAPS fall within the 1–10 nm range and were mostly concentrated around 1.5 and 3.5 nm (Figure 4a,b). Only *T. fortunei* did not show any variation in micropore size distribution among woody IAPS (Figure 4a), having a similar trend to herbaceous-derived biochars. Among herbaceous IAPS-derived biochars, only those of *L. grandiflora* and *S. gigantea* displayed similar trends to woody ones, more specifically to those of *A. altissima*, while *R. japonica*, *P. lobata*, and *A. verlotiorum* did not show a variation in the reported size range (Figure 4b).

Macropores concentrated around the same area range in woody and herbaceous IAPS-derived biochars, specifically at 20 and 200 μm² (Figure 4c,d). On average, woody IAPS had a higher number of macropores at the 20 μm² area peak compared to herbaceous ones, and *T. fortunei* displayed less variation (Figure 4c). Among herbaceous-derived biochar, only *S. gigantea* had a comparable number of pores to woody IAPS at 20 μm²; however, considering the peak at 200 μm², herbaceous-derived biochars had a greater number of pores compared to woody ones; in particular, *L. grandiflora* and *R. japonica* had the highest number of pores (Figure 4d), and among woody IAPS, *A. altissima* had the highest number (Figure 4c).

The porous structure of the analyzed biochar was also visible in SEM images (Figure 5a–j). At the 1000× magnification, a honeycomb-like structure was visible, highlighting the remnants of the plant's vascular system.

FIGURE 3 Fourier infrared spectroscopy spectra of the 10 invasive alien plant species-derived biochars. The red lines indicate the biomass spectra, and the black ones indicate the biochar ones. Specific functional groups are indicated.



Qualitatively, it is possible to see that some woody IAPS-derived biochars have a higher concentration of small pores compared to herbaceous ones, whose pores are bigger (for example, [Figure 5d](#), *Q. rubra*, and [Figure 5f](#), *A. verlotiorum*), according to macropore size distribution analysis ([Figure 4c,d](#)). Interestingly, here too, it is possible to see that *S. gigantea* derived biochar had a high concentration of small pores ([Figure 5j](#)).

3.3 | Principal component analysis

The two first components (PC1 and PC2) of the PCA explained 79% of the dataset's total variance, with PC1 and

PC2 explaining respectively 56% and 23% ([Figure 6a,b](#)). All variables were significantly correlated to PC1, except for CEC ([Table 1](#)). Among these, pH, N, Ca, K, Mg, P, ash, volatile, moisture contents, and yield were strongly positively correlated with PC1, while SA, C, H, O, fixed C, $H:C_{org}$, $O:C_{org}$, and the Pb^{2+} adsorption capacity correlated negatively with PC1. The variables that correlate positively with PC2 are SA, C, H, O, Fixed C, $H:C_{org}$, $O:C_{org}$, and Pb^{2+} adsorption, as opposed to pH, CEC, Ca, K, Mg, P, N, ash, volatiles, and moisture content, which correlated negatively, while yield did not correlate to PC2 ([Table 1](#)). PC1 separates well among the two growth forms, with herbaceous IAPS having higher values on PC1, contrary to woody ones ([Figure 6a](#)).

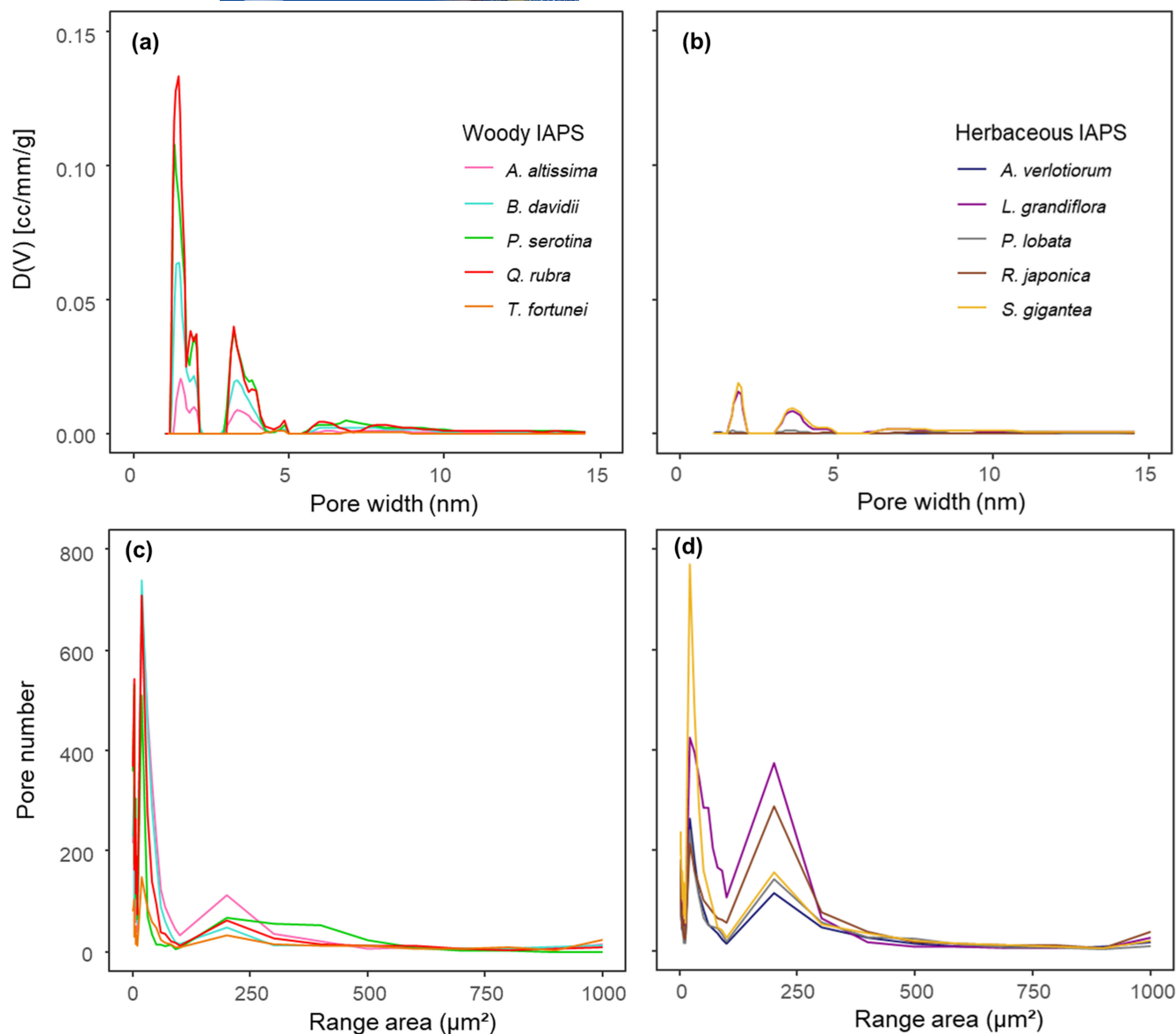


FIGURE 4 Pore size distribution analysis; panels (a, b) represent the micropore size distribution of the IAPS-derived biochar estimated via the density functional theory approach on the Brunauer–Emmett–Teller (BET) isotherm for woody (a) and herbaceous (b) IAPS. Panels (c, d) represent the frequency of pores per area range for woody and herbaceous species, respectively. IAPS, invasive alien plant species.

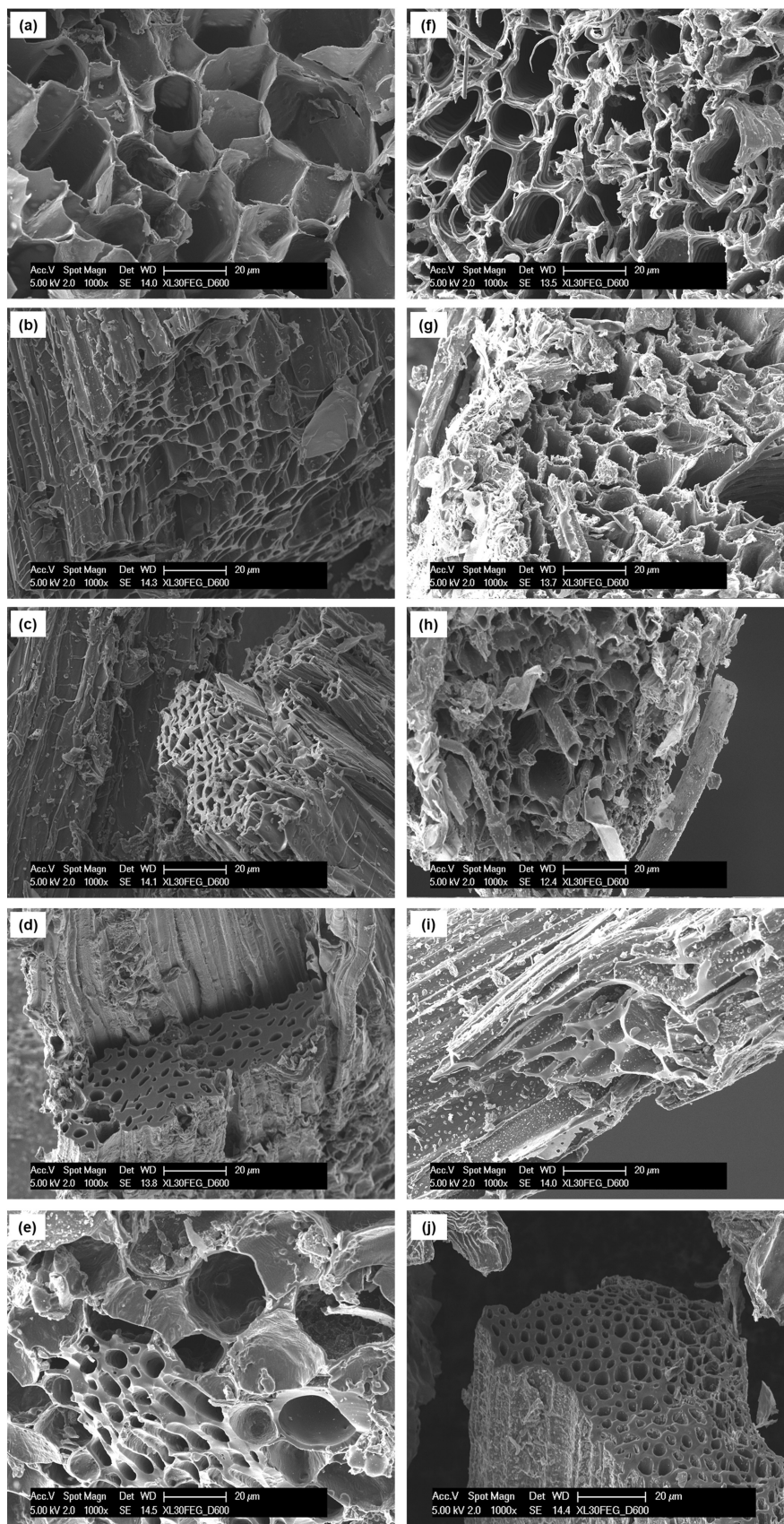
4 | DISCUSSION

4.1 | IAPS' biochar for soil amendment purposes

Biochar application can improve the soil's chemical-physical characteristics in terms of increasing organic matter, pH, electrical conductivity, total nutrients, CEC, water-holding capacity, and microbial activity, as well as plant above- and below-ground biomass production, influencing root architectural characteristics (Ahmad et al., 2014; Amendola et al., 2017; Basso et al., 2013; Cornelissen et al., 2013; Laghari et al., 2015; Montagnoli et al., 2021; Novak et al., 2009; Vaccari et al., 2011). The

10 IAPS-derived biochars showed comparable properties to those derived from more traditional feedstocks produced under similar conditions, for example, measured yields (Ferraro et al., 2021; Tu et al., 2022), pH (Becagli et al., 2022; Nandillon, Lebrun, et al., 2019; Nandillon, Miard, et al., 2019; Ronsse et al., 2013), nutrient content (Ippolito et al., 2020), and CEC (Tu et al., 2022). Overall, our results suggest that all 10 IAPS-derived biochars have promising characteristics for potential applications as soil amendments. However, we found significant differences among the selected IAPS and between the two growth forms, which can be ascribed to the differences in feedstock chemical composition (lignin, hemicellulose, cellulose, and organic compounds) that respond

FIGURE 5 Scanning electron microscopy image at 1000 \times of woody IPAS-derived biochar (left panel) and herbaceous IAPS-derived biochar (right panel). *Ailanthus altissima* (a), *Buddleja davidii* (b), *Prunus serotina* (c), *Quercus rubra* (d), and *Trachycarpus fortunei* (e), *Artemisia verlotiorum* (f), *Ludwigia grandiflora* (g), *Pueraria lobata* (h), *Reynoutria japonica* (i), and *Solidago gigantea* (j). The line represents 20 μm .



differently to the pyrolysis process (Keiluweit et al., 2010; Wang et al., 2021). In line with previous findings (Blanco-Canqui, 2017; Enders et al., 2012; Yuan et al., 2011), our

results suggest that herbaceous IAPS-derived biochars are characterized by high pH values and nutrient content (N, Ca, K, Mg, and P), which are optimal properties for

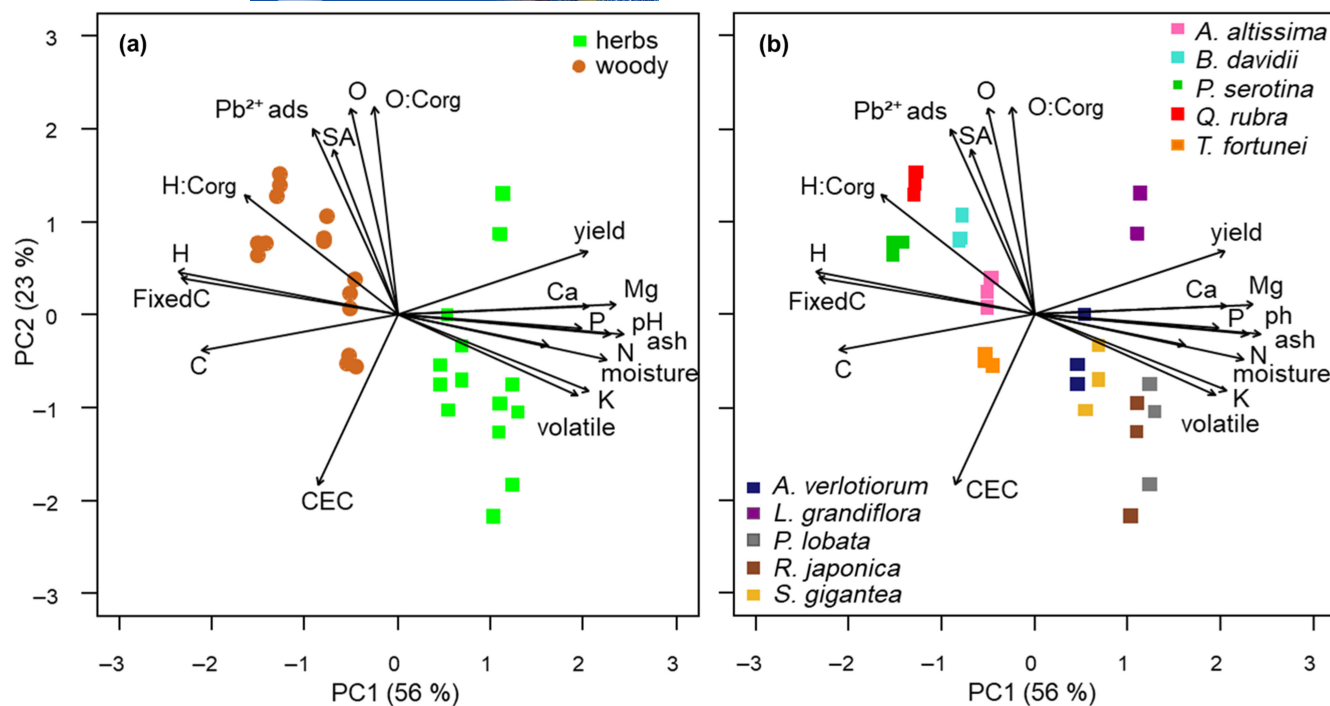


FIGURE 6 Principal component analysis, encompassing all the variables analyzed to characterize biochar properties as soil amendment, remediation, and carbon storage.

soil amendment since they are limiting factors for plant growth (e.g., Moreau et al., 2019). In particular, biochar's alkaline properties are relevant for nutrient adsorption and microbial biomass; however, different effects have been observed according to initial soil conditions; for example, it has been observed that biochar incorporation in soils had effects in terms of plant-available P in acidic/neutral soils, whereas no significant effects were observed in alkaline soils (Ding et al., 2016; Ortiz et al., 2020). Our results suggest that *P. lobata*-derived biochar might be considered the most promising feedstock for the production of biochar devoted to soil amendment applications, having the highest pH and macronutrient content.

Although we found a wide range of SAs for the 10 IAPS-derived biochars, the woody species-derived biochars showed higher values than the herbaceous, probably due to the higher microporosity where many smaller pores increase the SA (Ferraro et al., 2021; Ippolito et al., 2020). Herbaceous IAPS-derived biochars had a higher number of larger pores, which might relate to the morphological structure of the feedstock, as observed in the SEM images, and to its lower density (Leng et al., 2021; Sparavigna, 2022; Werdin et al., 2020). Hence, herbaceous IAPS-derived biochar may be more suitable for soil water availability and aeration (Ippolito et al., 2020), as an abundant number of large pores helps overcome the capillary forces that instead hold water in the smaller-sized pores of woody IAPS-derived biochar (Weber & Quicker, 2018). Some of the biomass characteristics could also be phylogenetically

related since species of the same taxon often share similar traits (Revell et al., 2008). Despite our dataset being too small to make conclusions about trait phylogenetic conservatism that can result in similar biochar properties, we found that two IAPS that belong to the same family (Asteraceae family, *S. gigantea*, and *A. verlotiorum*) can have different structural and functional properties. This could also be related to the growth and climatic conditions of the IAPS, which might influence the biomass structure (e.g., differences in conductive tissues) and explain differences in the volume and SA of biochar's pores. Indeed, site-specific climatic and soil conditions directly influence the growth of plants and affect the anatomy and chemical composition of biomass. For example, woody species respond to drought conditions by decreasing the conduit diameter and thickening the cell wall (Li et al., 2023). These conditions could be translated to the biochar structure, since higher lignin contents in feedstock result in greater SA and porosity of biochar (Leng et al., 2021).

4.2 | Soil remediation potential

Most of the research on IAPS-derived biochar focused on its bioremediation potential, suggesting that it is as effective as traditional feedstocks (Feng et al., 2021; Lian et al., 2020; Nandillon, Lebrun, et al., 2019; Nandillon, Miard, et al., 2019). Our results corroborate previous findings (Chi et al., 2017; Fan et al., 2019) and highlight that

TABLE 1 Pearson's correlation coefficients (r) and level of significance (p) between the first two axes of the principal component analysis (PC1 and PC2) and the variables measured on the IAPS-derived biochars.

| Variables | PCA axis | |
|----------------------|----------|----------|
| | PC1 | PC2 |
| pH | 0.93*** | -0.63*** |
| CEC | ns | -0.73*** |
| SA | -0.61*** | 0.75*** |
| Ca | 0.84*** | -0.50* |
| K | 0.87*** | -0.72*** |
| Mg | 0.95*** | -0.57*** |
| P | 0.81*** | -0.54** |
| C | -0.86*** | 0.43* |
| H | -0.97*** | 0.71*** |
| N | 0.92*** | -0.68*** |
| O | -0.68*** | 0.91*** |
| Fixed C | -0.95*** | 0.68*** |
| H:C _{org} | -0.79*** | 0.74*** |
| O:C _{org} | -0.63*** | 0.91*** |
| Pb ²⁺ ads | -0.72*** | 0.86*** |
| Ash | 0.99*** | -0.67*** |
| Volatile | 0.83*** | -0.70*** |
| Moisture | 0.66*** | -0.49** |
| Yield | 0.83*** | ns |

Abbreviations: CEC, cation exchange capacity; IAPS, invasive alien plant species; PCA, principal component analysis; SA, surface area.

* $p < .05$. ** $p < .01$. *** $p < .001$.

the lead (Pb²⁺) adsorption of biochar derived from woody IAPS is higher than that of herbaceous ones.

Many mechanisms are involved in heavy metal adsorption: interactions of electrostatic attraction, ion exchange, physical adsorption, surface complexation, and/or precipitation (Feng et al., 2021). Insights into surface functional groups prove helpful in assessing IAPS-derived biochars adsorption mechanisms. The FT-IR spectra showed peaks at 1380 and 1118 cm⁻¹, that are associated with -CH₂ and C-O vibrations, respectively (Liu et al., 2022). Different peaks in the 900–750 cm⁻¹ range indicate aromatic C-H out-of-plane deformation (Mireles et al., 2019). Peaks at 1700 and 1600 cm⁻¹ are associated respectively with carbonyl bonds (C=O), indicating the presence of carboxylic groups and possibly traces of aldehydes, ketones, and esters, and with aromatic C=C stretching (Granados et al., 2022), at 1593 cm⁻¹, the C=O could be due to the stretching of the aromatic ring in lignin (Fan et al., 2019). At 1420 cm⁻¹, the peak might be due to inorganic CO₃²⁻ (Fan et al., 2019). Hence, Pb²⁺ removal may be attributed to the coordination with π electrons of C=C functional

groups and precipitation with inorganic anions such as CO₃²⁻ (Chi et al., 2017). The oxygenated chemical groups could explain O's positive correlation on the second principal component (PC2), along with SA and Pb²⁺ removal efficacy, supporting that biochar SA is relevant for soil contaminant retention (Ippolito et al., 2020). Our results suggest that the differences in Pb²⁺ adsorption between woody and herbaceous-derived biochars could be explained by the different SAs, morphologies, and chemical compositions. Indeed, acidic and basic functional groups, respectively, reduce and increase during pyrolysis (Abdelhafez & Li, 2016; Shaaban et al., 2013), influencing biochar pH, which may in turn affect the solution's pH and the derived solubility (Fan et al., 2019).

Studies have also focused on the biochar adsorption of organic pollutants. Since C-O, C=O, and C=C groups can be effective in removing organic pollutants (Liu et al., 2022; Zhang et al., 2018) we can suppose that the biochar we produced may also have a potential in the remediation of organic pollutants. Also, biochar can create ecological niches for soil microorganisms, stimulating their growth, pollutant degradation (Brewer et al., 2014), and mineralization (Ni et al., 2020). Therefore, biochar could be used in polluted soils in combination with other practices, such as mulching, that promote the growth of the microbial community (Dalle Fratte et al., 2022). However, it is important to note that soil metal pollution is often in the polymetallic form; therefore, biochar addition may have different effects according to the pollutant's combination. For instance, biochar application increases the soil pH, simultaneously reducing and increasing the mobility of Pb and As, respectively, since the latter is mainly present in the oxyanion form (Nandillon, Lebrun, et al., 2019; Nandillon, Miard, et al., 2019).

4.3 | Biochar stability and climate change mitigation potential

Biochar stability is relevant for carbon sequestration, contributing to reducing greenhouse gas emissions (Leng et al., 2019). In our work, biochar stability and its stable carbon content (Leng et al., 2019) were evaluated through the analysis of the molar ratios (H:C_{org} and O:C_{org}) and fixed carbon, that is, the carbon content that remains in the solid structure after the volatile components are driven off (Weber & Quicker, 2018).

Biochar from woody IAPS was more stable in terms of carbon, than herbaceous ones, showing higher values of fixed carbon content (Ghysels et al., 2022; Leng et al., 2019), which could be expected by the higher lignin content (Windeatt et al., 2014). The lower fixed carbon content of the herbaceous IAPS is due to the higher

volatile components, which are in turn related to both labile carbon (Leng et al., 2019) and ash content (Enders et al., 2012; Windeatt et al., 2014), as also highlighted by our results. In particular, H:C represents the aromaticity of biochar directly proportional to its resistance to biological degradation and, thus, to its stability (Lehmann & Joseph, 2015). When observing our H:C_{org} results, all 10 IAPS-derived biochars had values well under 0.7, meaning more fused aromatic rings and thermochemically altered structures (Ippolito et al., 2020), consistent with our FT-IR results, which show an abundance of double carbon bonding. The thermochemical alteration can be monitored from the thermal decomposition of cellulose, hemicellulose, and lignin by the disappearance of the band at 1000 cm⁻¹ in the spectra of the biochar assigned to C–O and C–C stretching or C–OH bending, which is prominent in the feedstock ones (Ferraro et al., 2021).

The O:C_{org} results were all below the 0.2 value indicating a half-life greater than 1000 years (Ippolito et al., 2020), but herbaceous IAPS on average possess lower values, this was also true for the H:C ratio.

Surprisingly, these findings suggest that herbaceous species are more stable than woody ones, contrary to what was observed for fixed carbon. It is important to note that the molar ratios are not always accurate in predicting biochar stability, and contrasting results can be found in the literature (Bartoli et al., 2022; Enders et al., 2012; Tu et al., 2022). There might be a relevant fraction of O bound to inorganic compounds such as K, Na, Ca, Mg oxides, and phosphates that undergo thermal decomposition between 500 and 600°C, contributing to the reduction of the O:C ratio in this temperature range (Tan & Lagerkvist, 2011), supporting the idea that high ash contents might affect the interpretation of the molar ratios despite the correction for carbonates (Enders et al., 2012). Only considering the molar ratios or fixed carbon content to estimate biochar stability might not be enough. For this reason, Enders et al proposed that the molar ratios should be considered along with the volatile matter content. Our results had a volatile matter below 80%, an O:C_{org} ratio below 0.2, and an H:C_{org} below 0.4, which indicates high C sequestration potential (Spokas, 2010). Considering the negative correlations the three biochar stability indicators have to PC1, the negative side of the axis may be indicative of high carbon stability that is where biochar from woody IAPS is distributed, and it can be extrapolated that biochars derived from woody IAPS may be more stable in virtue of the higher fixed carbon. Although IAPS-derived biochar showed relevant properties in different fields of application, we found a clear trade-off between biochars with the potential for carbon storage and climate change mitigation (negative PC1 values) and biochars with high soil amendment potential (positive PC1 values), suggesting that two different

preferential uses could be made with the biomasses of woody and herbaceous IAPS, respectively. The biochar's metal adsorption potential (higher PC2 values) constitutes an independent axis of variation, which may relate to the biochar pores size and thus to the structure of IAPS biomass tissues.

5 | CONCLUSIONS

Invasive alien plant species biomass derived from eradication measures is considered waste material according to the current legislation. Finding innovative techniques to valorize these biomasses is crucial for creating a win-win situation, turning waste into a resource by following circular economy principles, and further implementing IAPS management practices. According to our results, the analyzed IAPS biomasses derived from eradication measures are suitable as feedstock for biochar production, which resulted optimal for different fields of application such as soil amendment, phytoremediation, and carbon stock, when, compared to more traditional feedstocks.

Herbaceous IAPS-derived biochar showed higher affinities for soil amendment applications (higher pH, higher macronutrient contents), while woody IAPS-derived biochar had great potential in terms of carbon stability and heavy metal adsorption. However, all 10 IAPS-derived biochars were highly stable and all had considerable carbon sequestration potential. Finally, we highlighted that for an optimal and correct application of these biochars to soils, to avoid unexpected effects compared to the characteristics of biochar alone, it is fundamental first and foremost to acquire the specificity of soil complex chemical–physical characteristics conditions (nutrient, pH, type of pollutant).

AUTHOR CONTRIBUTIONS

Alex Ceriani: Data curation; formal analysis; visualization; writing – original draft; writing – review and editing. **Michele Dalle Fratte:** Formal analysis; validation; writing – review and editing. **Gustavo Agosto:** Data curation; formal analysis. **Peter Beatrice:** Formal analysis; writing – review and editing. **Marcella Reguzzoni:** Writing – review and editing. **Lorenzo Bettucci:** Writing – review and editing. **David Casini:** Writing – review and editing. **Bruno Enrico Leone Cerabolini:** Conceptualization; funding acquisition; writing – review and editing. **Antonio Montagnoli:** Conceptualization; funding acquisition; writing – review and editing.

ACKNOWLEDGMENTS

We wish to thank Giulia Lotti from Re-Cord for her precious help at the company's laboratory and Alessio Miali and Marco Conti for their help in collecting samples.

Alex Ceriani is a Ph.D. student in the Life Sciences and Biotechnology course at the University of Insubria, funded by the NOP PhD programs on green topics of the Italian Ministry of University and Research (MUR), while Michele Dalle Fratte was funded by Fondazione Lombardia per l'Ambiente (FLA).

CONFLICT OF INTEREST STATEMENT

The authors declare no conflicts of interest.

DATA AVAILABILITY STATEMENT

The data that support the findings of this study are available in zenodo at <https://doi.org/10.5281/zenodo.10184814>.

ORCID


Alex Ceriani  <https://orcid.org/0009-0007-9470-3063>

Michele Dalle Fratte  <https://orcid.org/0000-0002-7907-1586>

Peter Beatrice  <https://orcid.org/0000-0001-8331-8273>

Marcella Reguzzoni  <https://orcid.org/0000-0003-3738-6632>

Lorenzo Bettucci  <https://orcid.org/0009-0009-5804-6654>

David Casini  <https://orcid.org/0000-0002-8106-2611>

Bruno Enrico Leone Cerabolini  <https://orcid.org/0000-0002-3793-0733>

Antonio Montagnoli  <https://orcid.org/0000-0002-8921-0754>

REFERENCES

- Abdelhafez, A. A., & Li, J. (2016). Removal of Pb(II) from aqueous solution by using biochars derived from sugar cane bagasse and orange peel. *Journal of the Taiwan Institute of Chemical Engineers*, *61*, 367–375. <https://doi.org/10.1016/j.jtice.2016.01.005>
- Ahmad, M., Moon, D. H., Vithanage, M., Koutsospyros, A., Lee, S. S., Yang, J. E., Lee, S. E., Jeon, C., & Ok, Y. S. (2014). Production and use of biochar from buffalo-weed (*Ambrosia trifida* L.) for trichloroethylene removal from water. *Journal of Chemical Technology and Biotechnology*, *89*(1), 150–157. <https://doi.org/10.1002/jctb.4157>
- Amalina, F., Razak, A. S. A., Krishnan, S., Sulaiman, H., Zularisam, A. W., & Nasrullah, M. (2022). Biochar production techniques utilizing biomass waste-derived materials and environmental applications – A review. *Journal of Hazardous Materials Advances*, *7*, 100134. <https://doi.org/10.1016/j.hazadv.2022.100134>
- Amendola, C., Montagnoli, A., Terzaghi, M., Trupiano, D., Oliva, F., Baronti, S., Miglietta, F., Chiatante, D., & Scippa, G. S. (2017). Short-term effects of biochar on grapevine fine root dynamics and arbuscular mycorrhizae production. *Agriculture, Ecosystems and Environment*, *239*, 236–245. <https://doi.org/10.1016/j.agee.2017.01.025>
- Barney, J. N., Tekiela, D. R., Dollete, E. S., & Tomasek, B. J. (2013). What is the 'real' impact of invasive plant species? *Frontiers in Ecology and the Environment*, *11*(6), 322–329. <https://doi.org/10.1890/120120>
- Baronti, S., Magno, R., Maienza, A., Montagnoli, A., Ungaro, F., & Vaccari, F. P. (2022). Long term effect of biochar on soil plant water relation and fine roots: Results after 10 years of vineyard experiment. *Science of the Total Environment*, *851*, 158225. <https://doi.org/10.1016/j.scitotenv.2022.158225>
- Bartoli, M., Troiano, M., Giudicianni, P., Amato, D., Giorcelli, M., Solimene, R., & Tagliaferro, A. (2022). Effect of heating rate and feedstock nature on electrical conductivity of biochar and biochar-based composites. *Applications in Energy and Combustion Science*, *12*, 100089. <https://doi.org/10.1016/j.jaacs.2022.100089>
- Basso, A. S., Miguez, F. E., Laird, D. A., Horton, R., & Westgate, M. (2013). Assessing potential of biochar for increasing water-holding capacity of sandy soils. *GCB Bioenergy*, *5*, 132–143. <https://doi.org/10.1111/gcbb.12026>
- Becagli, M., Arduini, I., & Cardelli, R. (2022). Using biochar and vermiwash to improve biological activities of soil. *Agriculture*, *12*, 178. <https://doi.org/10.3390/agriculture12020178>
- Bisi, F., Montagnani, C., Cardarelli, E., Manenti, R., Trasforini, S., Gentili, R., Ardenghi, N. M. G., Citterio, S., Bogliani, G., Ficotola, F., Rubolini, D., Puzzi, C., Norcini, A., Scelsi, F., Rampa, A., Rossi, E., Grande, D., Mazzamuto, M. V., Wauters, L. A., & Martinoli, A. (2018). *Strategia di azione e degli interventi per il controllo e gestione delle specie alloctone*. Documento aggiornato da Regione Lombardia (versione novembre 2022).
- Blanco-Canqui, H. (2017). Biochar and soil physical properties. *Soil Science Society of America Journal*, *81*, 687–711. <https://doi.org/10.2136/sssaj2017.01.0017>
- Bolpagni, R. (2021). Towards global dominance of invasive alien plants in freshwater ecosystems: The dawn of the Exocene? *Hydrobiologia*, *848*(9), 2259–2279. <https://doi.org/10.1007/s10750-020-04490-w>
- Borokini, T., & Babalola, F. (2012). Management of invasive plant species in Nigeria through economic exploitation: Lessons from other countries. *Management of Biological Invasions*, *3*(1), 45–55. <https://doi.org/10.3391/mbi.2012.3.1.05>
- Brewer, C. E., Chuang, V. J., Masiello, C. A., Gonnermann, H., Gao, X., Dugan, B., Driver, L. E., Panzacchi, P., Zygourakis, K., & Davies, C. A. (2014). New approaches to measuring biochar density and porosity. *Biomass and Bioenergy*, *66*, 176–185. <https://doi.org/10.1016/j.biombioe.2014.03.059>
- Carson, B. D., Lishawa, S. C., Tuchan, N. C., Monks, A. M., Lawrence, B. A., & Albert, D. A. (2018). Harvesting invasive plants to reduce nutrient loads and produce bioenergy: An assessment of Great Lakes coastal wetlands. *Ecosphere*, *9*, e02320. <https://doi.org/10.1002/ecs2.2320>
- Ceriani, A., Dalle Fratte, M., Agosto, G., Montagnoli, A., & Cerabolini, B. E. L. (2023). Using plant functional traits to define the biomass energy potential of invasive alien plant species. *Plants*, *12*, 3198. <https://doi.org/10.3390/plants12183198>
- Chi, T., Zuo, J., & Liu, F. (2017). Performance and mechanism for cadmium and lead adsorption from water and soil by corn straw biochar. *Frontiers of Environmental Science & Engineering*, *11*(2), 15. <https://doi.org/10.1007/s11783-017-0921-y>
- Cornelissen, G., Martinsen, V., Shitumbanuma, V., Alling, V., Breedveld, G., Rutherford, D., Sparrevik, M., Hale, S., Obia, A., & Mulder, J. (2013). Biochar effect on maize yield and soil characteristics in five conservation farming sites in Zambia. *Agronomy*, *3*(2), 256–274. <https://doi.org/10.3390/agronomy3020256>

- Corton, J., Donnison, I. S., Patel, M., Bühle, L., Hodgson, E., Wachendorf, M., Bridgwater, A., Allison, G., & Fraser, M. D. (2016). Expanding the biomass resource: Sustainable oil production via fast pyrolysis of low input high diversity biomass and the potential integration of thermochemical and biological conversion routes. *Applied Energy*, 177, 852–862. <https://doi.org/10.1016/j.apenergy.2016.05.088>
- Dalle Fratte, M., Bolpagni, R., Brusa, G., Caccianiga, M., Pierce, S., Zanzottera, M., & Cerabolini, B. E. L. (2019). Alien plant species invade by occupying similar functional spaces to native species. *Flora*, 257, 151419. <https://doi.org/10.1016/j.flora.2019.151419>
- Dalle Fratte, M., Montagnoli, A., Anelli, S., Armiraglio, S., Beatrice, P., Ceriani, A., Lipreri, E., Miali, A., Nastasio, P., Enrico, B., & Cerabolini, L. (2022). Mulching in lowland hay meadows drives an adaptive convergence of above- and below-ground traits reducing plasticity and improving biomass: A possible tool for enhancing phytoremediation. *Frontiers in Plant Science*, 13, 1062911. <https://doi.org/10.3389/fpls.2022.1062911>
- Diagne, C., Leroy, B., Vaisière, A.-C., Gozlan, R. E., Roiz, D., Jarić, I., Salles, J.-M., Bradshaw, C. J. A., & Courchamp, F. (2021). High and rising economic costs of biological invasions worldwide. *Nature*, 592(67), 153–190. <https://doi.org/10.1038/s41586-021-03405-6>
- Dimitrova, A., Csilléry, K., Klisz, M., Lévesque, M., Heinrichs, S., Cailleret, M., Andivia, E., Madsen, P., Böhenius, H., Cvjetkovic, B., de Cuyper, B., de Dato, G., Fesus, P., Heinze, B., Ivetić, V., Köbölkuti, Z., Lazarević, J., Lazdina, D., Maaten, T., ... Montagnoli, A. (2022). Risks, benefits, and knowledge gaps of non-native tree species in Europe. *Frontiers in Ecology and Evolution*, 10, 908464. <https://doi.org/10.3389/fevo.2022.908464>
- Ding, Y., Liu, Y., Liu, S., Li, Z., Tan, X., Huang, X., Zeng, G., Zhou, L., & Zheng, B. (2016). Biochar to improve soil fertility. A review. *Agronomy for Sustainable Development*, 36, 36. <https://doi.org/10.1007/s13593-016-0372-z>
- Enders, A., Hanley, K., Whitman, T., Joseph, S., & Lehmann, J. (2012). Bioresource technology characterization of biochars to evaluate recalcitrance and agronomic performance. *Bioresource Technology*, 114, 644–653. <https://doi.org/10.1016/j.biortech.2012.03.022>
- Fan, L., Zhou, X., Liu, Q., Wan, Y., Cai, J., Chen, W., Chen, F., Ji, L., Cheng, L., & Luo, H. (2019). Properties of *Eupatorium adenophora* Spreng (Crofton weed) biochar produced at different pyrolysis temperatures. *Environmental Engineering Science*, 36, 937–946. <https://doi.org/10.1089/ees.2019.0028>
- Feng, Q., Wang, B., Chen, M., Wu, P., Lee, X., & Xing, Y. (2021). Invasive plants as potential sustainable feedstocks for biochar production and multiple applications: A review. *Resources, Conservation and Recycling*, 164, 105204. <https://doi.org/10.1016/j.resconrec.2020.105204>
- Ferraro, G., Pecori, G., Rosi, L., Bettucci, L., Fratini, E., Casini, D., Rizzo, A. M., & Chiaramonti, D. (2021). Biochar from lab-scale pyrolysis: Influence of feedstock and operational temperature. *Biomass Conversion and Biorefinery*, 1–11. <https://doi.org/10.1007/s13399-021-01303-5>
- Ghysels, S., Rathnayake, D., Maziarka, P., Masek, O., Sohi, S., & Ronsse, F. (2022). Biochar stability scores from analytical pyrolysis (Py-GC-MS). *Journal of Analytical and Applied Pyrolysis*, 161, 105412. <https://doi.org/10.1016/j.jaap.2021.105412>
- Granados, P., Mireles, S., Pereira, E., Cheng, C.-L., & Kang, J. J. (2022). Effects of biochar production methods and biomass types on lead removal from aqueous solution. *Applied Sciences*, 12(10), 5040. <https://doi.org/10.3390/app12105040>
- Haubrock, P. J., Turbelin, A. J., Cuthbert, R. N., Novoa, A., Taylor, N. G., Angulo, E., Ballesteros-Mejia, L., Bodey, T. W., Capinha, C., Diagne, C., Essl, F., Golivets, M., Kirichenko, N., Kourantidou, M., Leroy, B., Renault, D., Verbrugge, L., & Courchamp, F. (2021). Economic costs of invasive alien species across Europe. *NeoBiota*, 67, 153–190. <https://doi.org/10.3897/neobiota.67.58196>
- Ippolito, J. A., Cui, L., Kammann, C., Wrage-Mönnig, N., Estavillo, J. M., Fuertes-Mendizabal, T., Cayuela, M. L., Sigua, G., Novak, J., Spokas, K., & Borchard, N. (2020). Feedstock choice, pyrolysis temperature and type influence biochar characteristics: A comprehensive meta-data analysis review. *Biochar*, 2(4), 421–438. <https://doi.org/10.1007/s42773-020-00067-x>
- Kaushik, P., Pati, P. K., Khan, M. L., & Khare, P. K. (2022). Plant functional traits best explain invasive species' performance within a dynamic ecosystem – A review. *Trees, Forests and People*, 8, 100260. <https://doi.org/10.1016/j.tfp.2022.100260>
- Keiluweit, M., Nico, P. S., Johnson, M. G., & Kleber, M. (2010). Dynamic molecular structure of plant biomass-derived black carbon (biochar). *Environmental Science & Technology*, 44(4), 1247–1253. <https://doi.org/10.1021/es9031419>
- Laghari, M., Saffar, M., Hu, Z., Fazal, S., Xiao, B., Hu, M., Chen, Z., & Guo, D. (2015). Catena effects of biochar application rate on sandy desert soil properties and sorghum growth. *Catena*, 135, 313–320. <https://doi.org/10.1016/j.catena.2015.08.013>
- Lehmann, J., & Joseph, S. (Eds.). (2015). *Biochar for environmental management: Science, technology and implementation* (2nd ed.). Routledge. <https://doi.org/10.4324/9781849770552>
- Leng, L., Huang, H., Li, H., Li, J., & Zhou, W. (2019). Biochar stability assessment methods: A review. *Science of the Total Environment*, 647, 210–222. <https://doi.org/10.1016/j.scitotenv.2018.07.402>
- Leng, L., Xiong, Q., Yang, L., Li, H., Zhou, Y., Zhang, W., Jiang, S., Li, H., & Huang, H. (2021). An overview on engineering the surface area and porosity of biochar. *Science of the Total Environment*, 763, 144204. <https://doi.org/10.1016/j.scitotenv.2020.144204>
- Li, S., Lu, S., Wang, J., Chen, Z., Zhang, Y., Duan, J., Liu, P., Wang, X., & Guo, J. (2023). Responses of physiological, morphological and anatomical traits to abiotic stress in woody plants. *Forests*, 14, 91784. <https://doi.org/10.3390/f14091784>
- Lian, W., Yang, L., Joseph, S., Shi, W., Bian, R., Zheng, J., Li, L., Shan, S., & Pan, G. (2020). Bioresource technology utilization of biochar produced from invasive plant species to efficiently adsorb Cd (II) and Pb (II). *Bioresource Technology*, 317, 124011. <https://doi.org/10.1016/j.biortech.2020.124011>
- Liao, R., Gao, B., & Fang, J. (2013). Invasive plants as feedstock for biochar and bioenergy production. *Bioresource Technology*, 140, 439–442. <https://doi.org/10.1016/j.biortech.2013.04.117>
- Liu, X., Wang, Q., Song, X., Li, K., Ali, M., Wei, C., Che, J., Guo, S., & Dou, X. (2022). Utilization of biochar prepared by invasive plant species *Alternanthera philoxeroides* to remove phenanthrene co-contaminated with PCE from aqueous solutions. *Biomass Conversion and Biorefinery*, 1–14. <https://doi.org/10.1007/s13399-022-02720-w>
- Mathew, A. T., & Saravanakumar, M. P. (2022). Removal of micropollutants through bio-based materials as a transition to circular bioeconomy: Treatment processes involved, perspectives and bottlenecks. *Environmental Research*, 214(P4), 114150. <https://doi.org/10.1016/j.envres.2022.114150>

- Mireles, S., Parsons, J., Trad, T., Cheng, C.-L., & Kang, J. (2019). Lead removal from aqueous solutions using biochars derived from corn stover, orange peel, and pistachio shell. *International Journal of Environmental Science and Technology*, 16(10), 5817–5826. <https://doi.org/10.1007/s13762-018-02191-5>
- Montagnoli, A., Baronti, S., Alberto, D., Chiatante, D., Scippa, G. S., & Terzaghi, M. (2021). Pioneer and fibrous root seasonal dynamics of *Vitis vinifera* L. are affected by biochar application to a low fertility soil: A rhizobox approach. *Science of the Total Environment*, 751, 141455. <https://doi.org/10.1016/j.scitotenv.2020.141455>
- Monteiro, E., & Ferreira, S. (2022). Biomass waste for energy production. *Energies*, 15, 5943. <https://doi.org/10.3390/en15165943>
- Moreau, D., Bardgett, R. D., Finlay, R. D., Jones, D. L., & Philippot, L. (2019). A plant perspective on nitrogen cycling in the rhizosphere. *Functional Ecology*, 33, 540–552. <https://doi.org/10.1111/1365-2435.13303>
- Nackley, L. L., Lieu, V. H., Garcia, B. B., Richardson, J. J., Isaac, E., Spies, K., Rigdon, S., & Schwartz, D. T. (2013). Bioenergy that supports ecological restoration. *Frontiers in Ecology and Evolution*, 11, 535–540. <https://doi.org/10.1890/120241>
- Nandillon, R., Lebrun, M., Miard, F., Gaillard, M., Sabatier, S., Villar, M., Bourgerie, S., & Morabito, D. (2019). Capability of amendments (biochar, compost and garden soil) added to a mining technosol contaminated by Pb and As to allow poplar seed (*Populus nigra* L.) germination. *Environmental Monitoring and Assessment*, 191(7), 465. <https://doi.org/10.1007/s10661-019-7561-6>
- Nandillon, R., Miard, F., Lebrun, M., Gaillard, M., Sabatier, S., Bourgerie, S., Battaglia-Brunet, F., & Morabito, D. (2019). Effect of biochar and amendments on Pb and As phytotoxicity and phytoavailability in a technosol. *Clean – Soil Air Water*, 47, 1800220. <https://doi.org/10.1002/clen.201800220>
- Ni, N., Kong, D., Wu, W., He, J., Shan, Z., Li, J., Dou, Y., Zhang, Y., Song, Y., & Jiang, X. (2020). The role of biochar in reducing the bioavailability and migration of persistent organic pollutants in soil–plant systems: A review. *Bulletin of Environmental Contamination and Toxicology*, 104(2), 157–165. <https://doi.org/10.1007/s00128-019-02779-8>
- Novak, J. M., Busscher, W. J., Laird, D. L., Ahmedna, M., Watts, D. W., & Niandou, M. A. S. (2009). Impact of biochar amendment on fertility of a southeastern coastal plain soil. *Soil Science*, 174(2), 105–112. <https://doi.org/10.1097/SS.0b013e3181981d9a>
- Ortiz, R. L., Torres, E., Zalazar, D., Zhang, H., Rodriguez, R., & Mazza, G. (2020). Influence of pyrolysis temperature and bio-waste composition on biochar characteristics. *Renewable Energy*, 155, 837–847. <https://doi.org/10.1016/j.renene.2020.03.181>
- Pérez, G., Vilà, M., & Gallardo, B. (2022). Potential impact of four invasive alien plants on the provision of ecosystem services in Europe under present and future climatic scenarios. *Ecosystem Services*, 56, 101459. <https://doi.org/10.1016/j.ecoser.2022.101459>
- Peterson, B. G., Carl, P., Boudt, K., Bennett, R., Ulrich, J., Zivot, E., Cornilly, D., Hung, E., Lestel, M., Balkissoon, K., Wuertz, D., Christidis, A. A., Martin, R. D., Zhou, Z., & Shea, J. M. (2022). *PerformanceAnalytics: Econometric tools for performance and risk analysis*. R package version 1.4.3541. <https://CRAN.R-project.org/package=PerformanceAnalytics>
- Pyšek, P., Richardson, D. M., Rejmánek, M., Webster, G. L., Williamson, M., & Kirschner, J. (2004). Alien plants in checklists and floras: Towards better communication between taxonomists and ecologists. *Taxon*, 53, 131–143.
- R Core Team. (2022). *R: A language and environment for statistical computing*. R Foundation for Statistical Computing. <https://www.R-project.org/>
- Revell, L. J., Harmon, L. J., & Collar, D. C. (2008). Phylogenetic signal, evolutionary process, and rate. *Systematic Biology*, 57(4), 591–601. <https://doi.org/10.1080/10635150802302427>
- Revelle, W. (2023). *Psych: Procedures for psychological, psychometric, and personality research*. R package version 2.3.3. Northwestern University, Evanston, IL. <https://CRAN.Rproject.org/package=psych>
- Ronsse, F., van Hecke, S., Dickinson, D., & Prins, W. (2013). Production and characterization of slow pyrolysis biochar: Influence of feedstock type and pyrolysis conditions. *GCB Bioenergy*, 5(2), 104–115. <https://doi.org/10.1111/gcbb.12018>
- Schneider, C. A., Rasband, W. S., & Eliceiri, K. W. (2012). NIH image to ImageJ: 25 years of image analysis. *Nature Methods*, 9(7), 671–675. <https://doi.org/10.1038/nmeth.2089>
- Shaaban, A., Se, S. M., Mitan, N. M. M., & Dimin, M. F. (2013). Characterization of biochar derived from rubber wood sawdust through slow pyrolysis on surface porosities and functional groups. *Procedia Engineering*, 68, 365–371. <https://doi.org/10.1016/j.proeng.2013.12.193>
- Shapiro, S. S., & Wilk, M. B. (1965). An analysis of variance test for normality (complete samples). *Biometrika*, 52(3–4), 591–611. <https://doi.org/10.1093/biomet/52.3-4.591>
- Sherrod, L. A., Dunn, G., Peterson, G. A., & Kolberg, R. L. (2002). Inorganic carbon analysis by modified pressure-calcimeter method. *Soil Science Society of America Journal*, 66, 299–305. <https://doi.org/10.2136/sssaj2002.2990>
- Skjemstad, J. O., Gillman, G. P., Massis, A., & Spouncer, L. R. (2008). Measurement of cation exchange capacity of organic-matter fractions from soils using a modified compulsive exchange method. *Communications in Soil Science and Plant Analysis*, 39(5–6), 926–937. <https://doi.org/10.1080/00103620701881279>
- Sparavigna, A. C. (2022). Biochar for shape stabilized phase-change materials. chemrxiv.org. <https://doi.org/10.26434/chemrxiv-2022-4nthj>
- Spokas, K. A. (2010). Review of the stability of biochar in soils: Predictability of O:C molar ratios. *Carbon Management*, 1, 289–303. <https://doi.org/10.4155/cmt.10.32>
- Tan, Z., & Lagerkvist, A. (2011). Phosphorus recovery from the biomass ash: A review. *Renewable and Sustainable Energy Reviews*, 15, 3588–3602. <https://doi.org/10.1016/j.rser.2011.05.016>
- Tu, P., Zhang, G., Wei, G., Li, J., Li, Y., Deng, L., & Yuan, H. (2022). Influence of pyrolysis temperature on the physicochemical properties of biochars obtained from herbaceous and woody plants. *Bioresources and Bioprocessing*, 9, 131. <https://doi.org/10.1186/s40643-022-00618-z>
- Vaccari, F. P., Baronti, S., Lugato, E., Genesio, L., Castaldi, S., Fornasier, F., & Miglietta, F. (2011). Biochar as a strategy to sequester carbon and increase yield in durum wheat. *European Journal of Agronomy*, 34(4), 231–238. <https://doi.org/10.1016/j.eja.2011.01.006>
- Van Kleunen, M., Weber, E., & Fischer, M. (2010). A meta-analysis of trait differences between invasive and non-invasive plant species. *Ecology Letters*, 13, 235–245. <https://doi.org/10.1111/j.1461-0248.2009.01418.x>

- Velvizhi, G., Goswami, C., Shetti, N. P., Ahmad, E., Kishore Pant, K., & Aminabhavi, T. M. (2022). Valorisation of lignocellulosic biomass to value-added products: Paving the pathway towards low-carbon footprint. *Fuel*, *313*, 122678. <https://doi.org/10.1016/j.fuel.2021.122678>
- Wang, J., Zhao, M., Zhang, J., Zhao, B., Lu, X., & Wei, H. (2021). Characterization and utilization of biochars derived from five invasive plant species *Bidens pilosa* L., *Praxelis clematidea*, *Ipomoea cairica*, *Mikania micrantha* and *Lantana camara* L. for Cd²⁺ and Cu²⁺ removal. *Journal of Environmental Management*, *280*, 111746. <https://doi.org/10.1016/j.jenvman.2020.111746>
- Weber, K., & Quicker, P. (2018). Properties of biochar. *Fuel*, *217*, 240–261. <https://doi.org/10.1016/j.fuel.2017.12.054>
- Werdin, J., Fletcher, T. D., Rayner, J. P., Williams, N. S. G., & Farrell, C. (2020). Biochar made from low density wood has greater plant available water than biochar made from high density wood. *Science of the Total Environment*, *705*, 135856. <https://doi.org/10.1016/j.scitotenv.2019.135856>
- Windeatt, J. H., Ross, A. B., Williams, P. T., Forster, P. M., Nahil, M. A., & Singh, S. (2014). Characteristics of biochars from crop residues: Potential for carbon sequestration and soil amendment. *Journal of Environmental Management*, *146*, 189–197. <https://doi.org/10.1016/j.jenvman.2014.08.003>
- Yaashikaa, P. R., Kumar, P. S., Varjani, S., & Saravanan, A. (2020). A critical review on the biochar production techniques, characterization, stability and applications for circular bioeconomy. *Biotechnology Reports*, *28*, e00570. <https://doi.org/10.1016/j.btre.2020.e00570>
- Yuan, J., Xu, R., & Zhang, H. (2011). The forms of alkalis in the biochar produced from crop residues at different temperatures. *Bioresource Technology*, *102*(3), 3488–3497. <https://doi.org/10.1016/j.biortech.2010.11.018>
- Zanzottera, M., Dalle Fratte, M., Caccianiga, M., Pierce, S., & Cerabolini, B. E. L. (2021). Towards a functional phytosociology: The functional ecology of woody diagnostic species and their vegetation classes in northern Italy. *iForest*, *14*, 522–530. <https://doi.org/10.3832/ifer3730-014>
- Zhang, Z., Chen, L., Wang, J., Yao, J., & Li, J. (2018). Biochar preparation from: *Solidago canadensis* and its alleviation of the inhibition of tomato seed germination by allelochemicals. *RSC Advances*, *8*(40), 22370–22375. <https://doi.org/10.1039/c8ra03284j>

SUPPORTING INFORMATION

Additional supporting information can be found online in the Supporting Information section at the end of this article.

How to cite this article: Ceriani, A., Dalle Fratte, M., Agosto, G., Beatrice, P., Reguzzoni, M., Bettucci, L., Casini, D., Cerabolini, B. E. L., & Montagnoli, A. (2024). Woody and herbaceous invasive alien plant species-derived biochars are potentially optimal for soil amendment, soil remediation, and carbon storage. *GCB Bioenergy*, *16*, e13117. <https://doi.org/10.1111/gcbb.13117>